Bioorganic & Medicinal Chemistry 26 (2018) 1162–1166

Contents lists available at ScienceDirect

Bioorganic & Medicinal Chemistry

journal homepage: www.elsevier.com/locate/bmc

Synthesis and β-sheet propensity of constrained *N*-amino peptides

Matthew P. Sarnowski, Kyle P. Pedretty, Nicole Giddings, H. Lee Woodcock, Juan R. Del Valle *

Department of Chemistry, University of South Florida, Tampa, FL 33620, United States

ARTICLE INFO

Article history:
Received 29 June 2017
Revised 4 August 2017
Accepted 8 August 2017
Available online 31 August 2017

Keywords:
Peptidomimetics
Secondary structure
Amino acids
Peptide conformation
β-Strands

ABSTRACT

The stabilization of β-sheet secondary structure through peptide backbone modification represents an attractive approach to protein mimicry. Here, we present strategies toward stable β-hairpin folds based on peptide strand *N*-amination. Novel pyrazolidinone and tetrahydropyridazinone dipeptide constraints were introduced via on-resin Mitsunobu cyclization between α-hydrazino acid residues and a serine or homoserine side chain. Acyclic and cyclic *N*-amino peptide building blocks were then evaluated for their effect on β-hairpin stability in water using a GB1-derived model system. Our results demonstrate the strong β-sheet stabilizing effect of the peptide *N*-amino substituent, and provide useful insights into the impact of covalent dipeptide constraint on β-sheet folding.

1. Introduction

After α helices, β-sheets represent the most common secondary structure in proteins. A number of protein-protein and protein-DNA interactions implicated in pathogenesis involve β-sheets or strands at the macromolecular interface.[1] The β-sheet-like oligomerization and fibrilization of amyloid monomers, for example, is known to contribute to the progression of Alzheimer's and Parkinson's disease.[2] In cancer, Ras pathway hyperactivation relies, in part, on edge-edge interactions between the β-sheet domains of Ras and various downstream kinases.[3] Modulation of these and similar interactions with β-strand/sheet mimics has thus attracted considerable interest. Strategies aimed at stabilizing β-sheet conformations within shorter peptides have also played an important role in elucidating the anatomy and dynamics of biomolecular associations.[4]

Residues within parallel β-sheets are defined by ϕ and ψ dihedral angles close to −119° and 113°, respectively, whereas those in antiparallel β-sheets are at or near −139° and 135°.[1] In conjunction with *trans* amide (ω) bonds, these torsions result in a sawtooth amino acid arrangement featuring two H-bonding peptide 'edges' and two 'faces' harboring side chain functional groups. Enforcement of these backbone conformations has typically been achieved through judicious incorporation of sheet-forming side chains, covalent tethering approaches, turn-templated hairpin design, or the use of conformationally extended backbone isosteres.[1,5]

Our interest in β-strand/sheet stabilization led us to consider conformationally restricted peptidomimetic building blocks that could be readily incorporated into host structures. Ideally, these subunits would enforce extended dihedral angles, nucleate folding, and inhibit aggregation. Furthermore, we envisioned that an approach amenable to synthesis on solid support would enable the rapid conformational scanning of lead peptides.

We recently developed a class of peptidomimetics featuring a backbone *N*-amino substituent (Fig. 1).[6] This substituent provides a nucleophilic handle for subsequent covalent constraint and may engage in an intraresidue C6 H-bond. In addition to *N*-amino peptides (NAPs), our group reported a '*trans*-locked' (*R*)-tetrahydropyridazinedione (tpd) variant that results from covalent tethering of the *N*-amino substituent onto an adjacent aspartic acid side chain.[7] The current work introduces two novel peptidomimetics based on (*R*)-tetrahydropyridazinone (tpy) and (*R*)-pyrazolidinone (pyz) scaffolds (Fig. 1). These orthotic constraints are readily introduced on solid support via Mitsunobu reactions between an *N*-aminated residue and an adjacent D-homoserine or D-serine side chain. Engaging D-amino acid side chains in covalent tethering restricts the ψ dihedral angles to values close to those in β-sheets (+120°). Here, we also evaluate the β-sheet propensity of *N*-amino, tpd, tpy, and pyz constraints side-by-side in a biologically relevant model of β-hairpin folding using NMR.

2. Solution-phase synthesis

Model pyz and tpy constrained dipeptides were first synthesized in solution starting from D-serine and D-homoserine, respectively (Scheme 1). Following Alloc protection, the carboxylic acids

* Corresponding author.
E-mail address: delvalle@usf.edu (J.R. Del Valle).

http://dx.doi.org/10.1016/j.bmc.2017.08.017
0968-0896/

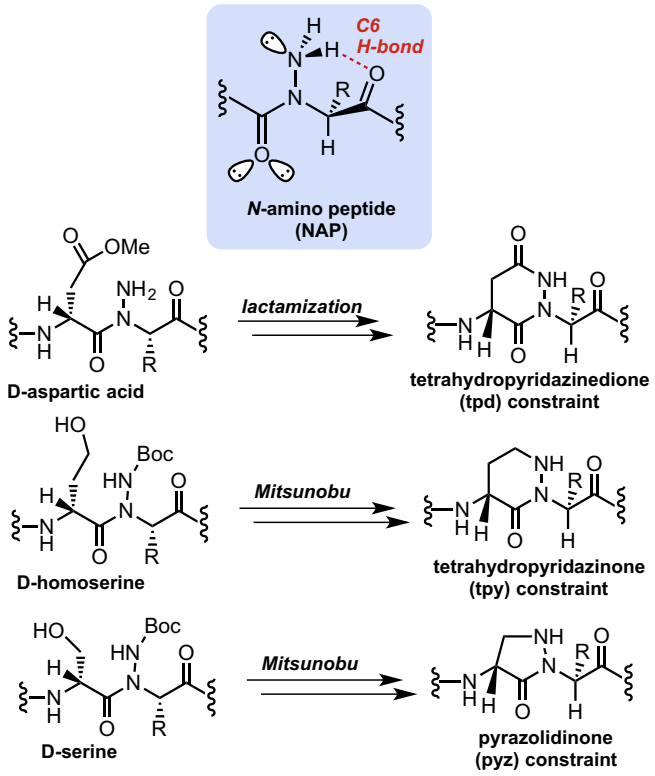

Fig. 1. Constrained *N*-amino peptides.

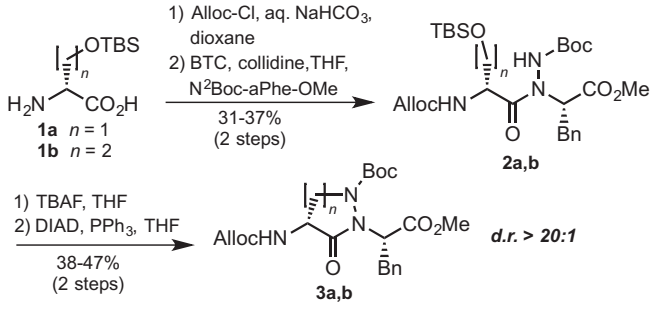

Scheme 1. Synthesis of constrained dipeptides in solution.

were converted to acid chlorides using BTC and condensed with H-(*N*^{2}-Boc)-aPhe-OMe. Silyl ether deprotection and intramolecular Mitsunobu cyclization yielded cyclic peptidomimetics **3a** and **3b** in good yield. The diastereopurity of intermediates **2a** and **2b** were determined to be >20:1 by comparison of their ^{1}H NMR spectra with those of diastereomeric (D-aPhe) analogs. The crude Mitsunobu reaction mixture of **3a** did not reveal any detectable elimination to dehydroalanine or epimerization at the configurationally labile D-Ser α-carbon. These results thus established feasibility, prompting us to adapt our covalent tethering approach to solid-phase peptide synthesis.

3. Design and synthesis of β-sheet model peptides

In order to experimentally assess the β-sheet propensity of our constrained motifs, we employed a 16-residue β-hairpin derived from the protein G immunoglobulin-binding domain B1 (GB1, Fig. 2).[8] GB1$_{41-56}$, a soluble monomeric antiparallel β-sheet model peptide featuring a 4-residue turn, is estimated to be ~40% folded in aqueous solution at 5 °C.[9] This peptide and its close analogs have

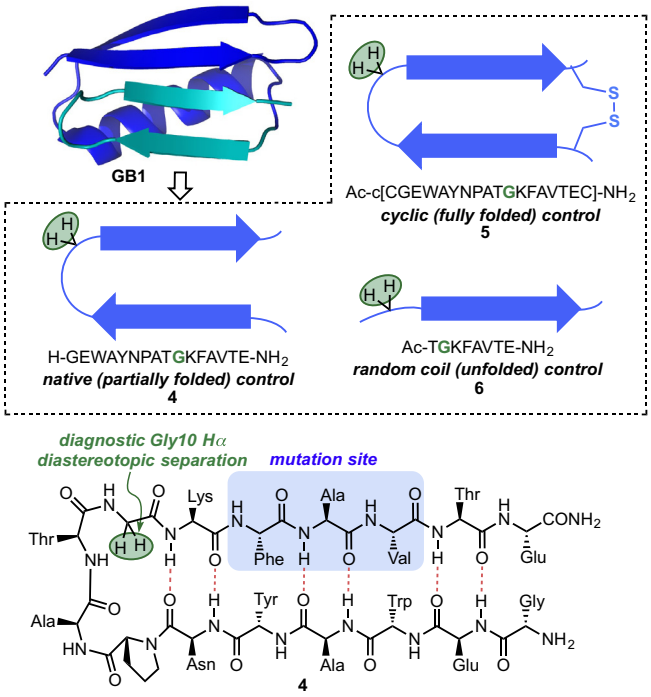

Fig. 2. Model β-hairpins for thermodynamic analysis. The green circle indicates the diagnostic Gly10Hα protons from which diastereotopic ^{1}H NMR separation values are derived. The tripeptide region targeted for mutation is highlighted in blue.

been utilized to evaluate the impact of various mutations on β-sheet stability.[10] Recently, Horne and co-workers introduced targeted mutations into the GB1$_{41-56}$ model peptide in order to enhance its folded population and facilitate chemical shift assignments.[10d] Our studies on the β-sheet propensity of constrained NAP derivatives make use of this sequence in conjunction with its cyclic (fully folded) and truncated (random coil) variants, as control peptides (**4**–**6**).

Previous work with hairpins related to **4** has demonstrated chemical shift separation of the diastereotopic Gly Hα protons within the turn to be diagnostic of folded population. This diastereotopic separation arises from the distinct chemical shift environment of each proton within a stable folded hairpin.[11] Conversely, destabilization of secondary structure leads to conformational averaging and coalescence of these signals. To evaluate our constraints, we targeted residues 12–14 as candidate sites for mutational analysis. This region was selected on the basis of its central position within the northern β-strand, and for ease of synthesis. Moreover, incorporation of a tpd, tpy, or pyz motif results in loss of the pro-(*S*) side chain, which may negatively impact folded population. We thus considered mutations at Ala13 to be the least disruptive given the low β-sheet propensity of alanine as measured in a full-length GB1 model system.[12]

Hydrazino acid derivatives **8a** and **8b** were prepared by oxaziridine-mediated electrophilic amination[13] of phenylalanine and valine as shown in Scheme 2. We previously reported a 2-step protocol to access these building blocks via α-amino ester amination.[14] The current method involves direct amination of the unprotected zwitterions in water, and gives pure products following trituration with Et_2O/hexanes. Assembly of peptides on solid support employed standard Fmoc chemistry, with the exception of coupling to *N*^{2}-Boc-protected hydrazino amides. In these cases, acid chloride activation was required. The configurationally stable Fmoc-Asp(Me)-Cl building block for tpd formation was pre-formed using $SOCl_2$, as described previously.[7] As in Scheme 1, Fmoc-(D)

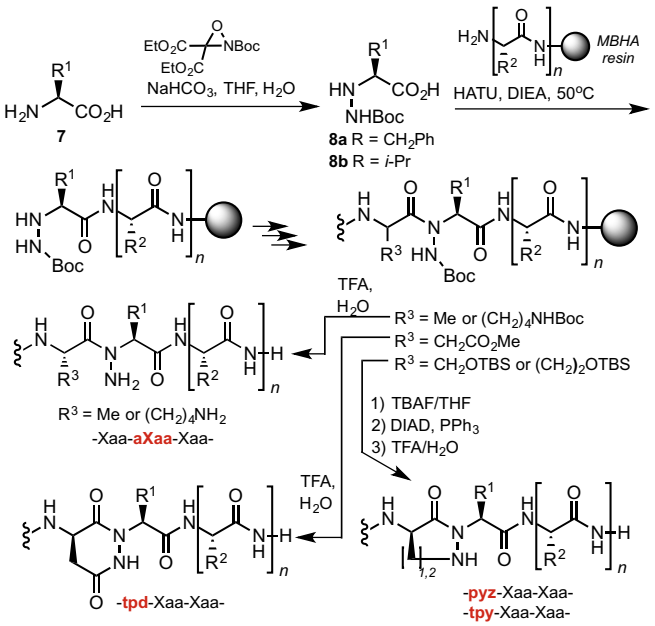

Scheme 2. Solid-phase synthesis of constrained NAPs.

hSer-OH[15]and Fmoc-(D)Ser-OH[16] were activated in situ with BTC/-collidine. Formation of the tpd ring occurred readily during cleavage from the resin with 95:5 TFA:H_2O. Mitsunobu cyclizations to produce tpy and pyz constraints were performed on resin, prior to global deprotection/cleavage. As the *N*-terminal Gly Fmoc group was not stable to DIAD/PPh_3 (due to base-mediated deprotection), these peptides were terminated with a Boc-protected Gly residue prior to Mitsunobu reactions.

Table 1 depicts each of the peptides synthesized for the current study. In addition to the native (unmutated) peptide **4**, we prepared its macrocyclic variant **5** (disulfide bridge) as a fully folded positive control. Truncated linear analog **6** was synthesized to provide Gly H α chemical shift separation values within a relevant random coil. Covalently constrained derivatives **9**–**11** display the orthotic bridge on the outer edge of the hairpin, so as not to interfere with interstrand H-bonding interactions. Compounds **12** and **13** are acyclic NAPs substituted at each of the outer edge amides within the region of interest. Finally, di-NAP mutant **14** was prepared to assess the impact of multiple backbone aminations, whereas *N*-methylated analog **15** allows for a comparison of NAP-based constraints with *N*-alkylation.

4. Structural and thermodynamic analysis

Detailed NMR studies of **9**–**15** were carried out at 1 mM concentration in D_2O (50 mM $NaHPO_4$, pH 6.8). ^1H NMR assignments were made on the basis of TOCSY and NOESY spectra obtained at 4 °C.

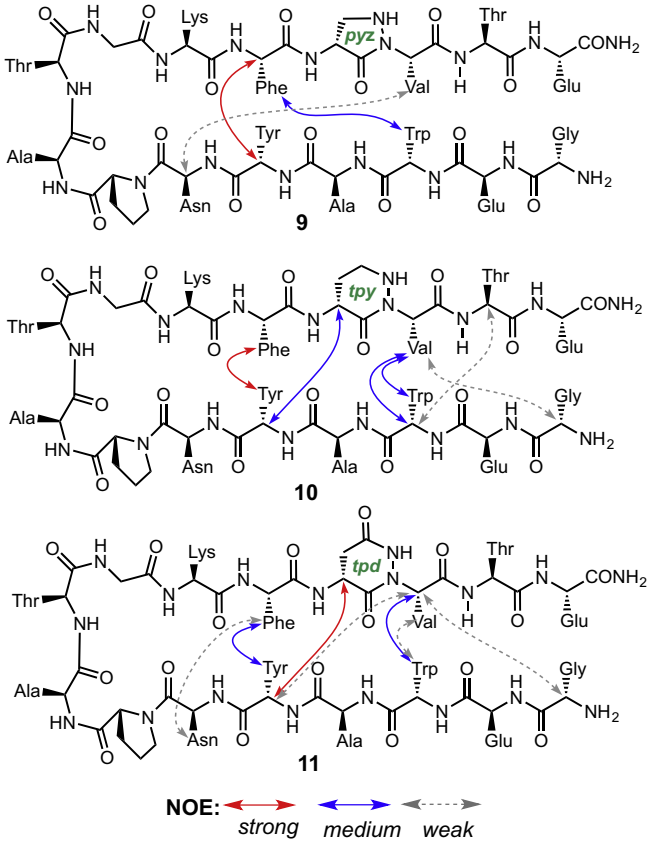

Fig. 3. Interstrand NOE correlations observed for **9**–**11**.

Examination of the NOESY spectra for each of the constrained NAPs revealed several key correlations indicative of folded structures. Fig. 3 depicts interstrand contacts observed for **9**–**11**. Notably, pyz mutant **9** exhibited few interstrand correlations relative to tpy and tpd mutants **10** and **11**. The α proton of the tpd and tpy residues, but not the pyz residue, engages in a close interaction with the Tyr5H α. Correlations between Trp3-Val14, Gly1-Val14, and Tyr5-Phe12 were also consistent in the spectra of **10** and **11**. These data qualitatively suggested enhanced stability of the tpy- and tpd-contaning β-hairpins relative to **9**.

In order to obtain a quantitative assessment of folding, we calculated the Gly_{10} Hα chemical shift separation for each peptide from TOCSY spectra (0.010 ppm uncertainty was assumed and error propagated for subsequent calculations). In our hands, the fully folded control peptide (**5**) and the random coil peptide (**6**) exhibited $\delta\Delta_{Gly10}$ values of 0.290 and 0.047 ppm, respectively. This dynamic range was used to calculate a folded fraction of 73% for the native (unmutated) peptide **4**, which is slightly higher than that previously reported (Table 2).[10d] The folded fraction of pyz

Table 1
Synthesized peptides.

Peptide	Sequence	HRMS m/z_{obs}	Yield %
4	H-GEWAYNPATGKFAVTE-NH_2	870.4214 $[M+2H]^{2+}$	25
5	Ac-c[CGEWAYNPATGKFAVTEC]-NH_2	993.9292 $[M+2H]^{2+}$	5
6	Ac-TGKFAVTEC-NH_2	893.4715 $[M+H]^{+}$	20
9	H-GEWAYNPATGKF-**pyz**-VTE-NH_2	876.9194 $[M+2H]^{2+}$	4
10	H-GEWAYNPATGKF-**tpy**-VTE-NH_2	883.9269 $[M+2H]^{2+}$	4
11	H-GEWAYNPATGKF-**tpd**-VTE-NH_2	890.9160 $[M+2H]^{2+}$	3
12	H-GEWAYNPATGK-**aPhe**-AVTE-NH_2	877.9276 $[M+2H]^{2+}$	9
13	H-GEWAYNPATGKFA-**aVal**-TE-NH_2	877.9280 $[M+2H]^{2+}$	15
14	H-GEWAYNPATGK-**aPhe**-A-**aVal**-TE-NH_2	885.4366 $[M+2H]^{2+}$	8
15	H-GEWAYNPATGK-(***N*-Me**)**Phe**-AVTE-NH_2	877.4299 $[M+2H]^{2+}$	21

Table 2
Folding thermodynamics of constrained NAPs.

Peptide	Mutation	$\Delta\delta Gly_{10}$ (ppm)	% Folded	ΔG_{fold} (kcal/mol)	$\Delta\Delta G_{fold}$ (kcal/mol)
4	native	0.224	73 ± 5	−0.5 ± 0.1	
9	pyz13	0.127	33 ± 5	+0.4 ± 0.1	+0.9
10	tpy13	0.171	51 ± 5	+0.0 ± 0.1	+0.5
11	tpd13	0.174	52 ± 5	+0.0 ± 0.1	+0.5
12	aPhe12	0.261	88 ± 6	−1.1 ± 0.3	−0.6
13	aVal14	0.252	84 ± 5	−0.9 ± 0.2	−0.4
14	aPhe12/aVal14	0.301	>99 ± 6	N/A	N/A
15	(*N*-Me)Phe12		24 ± 5	+0.6 ± 0.2	+1.1
15_{trans}	(*N*-Me)Phe12$_{trans}$	0.096	37 ± 5	+0.3 ± 0.1	+0.8
15_{cis}	(*N*-Me)Phe12 c_{is}	0.000			

mutant **9**, harboring a 5-membered ring constraint, was found to be only 33%, corresponding to destabilization of +0.9 kcal/mol relative to **4**. The tpy and tpd 6-membered ring constraints in **10** and **11** were better accommodated into the β-strand region, as these peptides were ~50% folded in water. *N*-Amino substitution without covalent tethering (**12** and **13**) resulted in a notable increase in β-hairpin population. The most dramatic stabilization of secondary structure was observed with the aPhe12/aVal14 double mutant (**14**). In this case, amination of two outer edge amides on the same β-strand yielded a fully folded acyclic β-hairpin. Conversely, backbone *N*-methylation in **15** resulted in +1.1 kcal/mol destabilization relative to **4** and +1.7 kcal/mol destabilization relative its *N*-amino counterpart **12**.

5. Computational analysis

In order to gain additional insights into the conformational preferences of NAP-based constraints, we carried out computational analysis on the model dipeptides shown in Fig. 4. Two-dimensional potential energy surfaces were computed as a function of backbone dihedral angles using CHARMM.[17] Subsequent constrained geometry optimizations were carried out with Q-Chem 4.4 at the ωB97X-D/6-31+G** level of theory.[18] NBO calculations were performed for each global minimum and additional points of interest to evaluate (de)stabilizing intramolecular interactions.[19]

Ramachandran plots for ϕ_{i+1}, ψ_{i+1} in **16** and **18** are shown in Fig. 5, with additional plots for cyclic NAPs (**18** and **19**) presented in the Supplementary Material. As noted above, idealized antiparallel β-sheets exhibit ϕ, ψ values in the −139°, 135° range. Examining the ϕ_{i+1}, ψ_{i+1} energy surfaces for **16**–**19** it becomes clear that **16** is more likely to adopt sheet-like conformations than **17**–**19**. Intuition would suggest this results from destabilizing clashes or ring strain that may occur in the cyclic NAPs, however this is not the case. Instead, the energy landscape of the ψ_{i+1} torsion in **17**–**19** is more accessible, allowing cyclic NAP derivatives to more easily adopt non-ideal conformations.

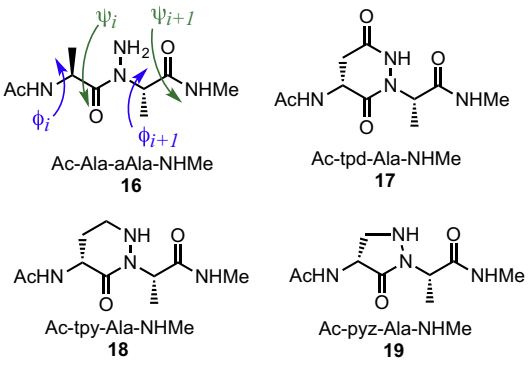

Fig. 4. Model dipeptides employed for computational analysis.

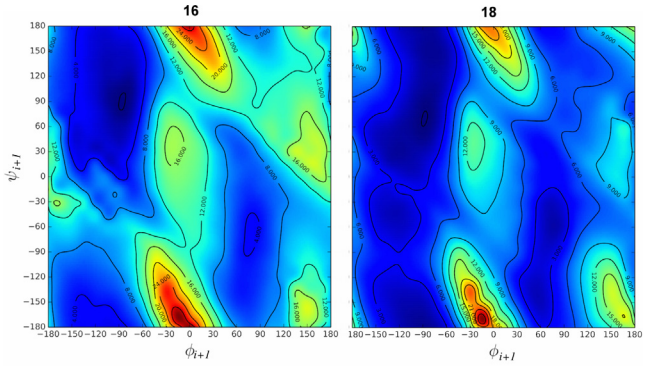

Fig. 5. Ramachandran plots for φ_{i+1}, ψ_{i+1} in **16** and **18**.

An additional critical factor appears to be the ability for the *N*-amino group to act either as a H-bond donor or acceptor. Examining structures with $\phi_{i+1} = -105°$, $\psi_{i+1} = -60°$ (i.e., the transition state ψ_{i+1} saddle point region in **16**) we found that cyclic NAPs **18** and **19** adopt stable geometries involving an H-bond between the C-terminal amide NH (donor) and the endocyclic *N*-amino nitrogen (acceptor). In contrast, the *N*-amino group in **16** acts only as a donor, avoiding stabilization of unproductive conformations (Fig. 6). NBO analysis on these structures reveals that the N···H—N interaction leads to stabilization gains in pyz, and tpy of 1.5, and 4.3 kcal/mol, respectively. While this cannot fully explain the experimental trends, it clearly illustrates that subtle stereoelectronic effects are playing a role in the conformational preferences of both cyclic and acyclic NAPs.

Lastly, we considered that the destabilization observed in hairpins **9**–**11** relative to **4** may be due to unfavorable ψ_i torsions within the heterocycles. Computational analysis of the ψ_i dihedral angles in **17**–**19** across a range of ϕ_i torsions showed a significant energetic cost associated with antiparallel β-sheet conformations. The ψ_i angle in the tpd and tpy rings of **17** and **18** are generally

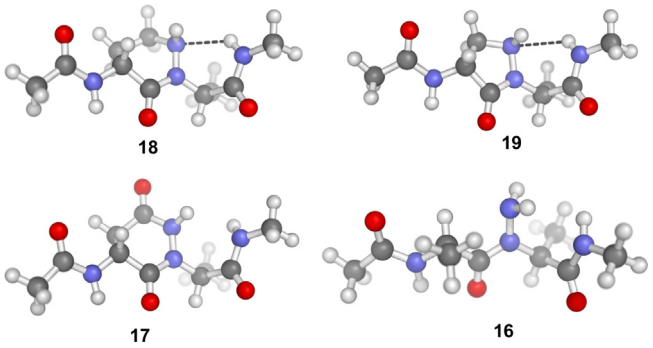

Fig. 6. Energy minimized structures of dipeptide models at $\phi_{i+1} = -105°$,$\psi_{i+1} = -60°$ showing stabilizing N···H—N interactions in **18** and **19**.

constrained to values well above 135°. Moreover, the lowest energy ϕ_i conformations in the cyclic NAP derivatives are in the +150° to 180° range. A ψ_i, ϕ_i dihedral energy scan of the more flexible acyclic NAP (**16**) revealed its ability to more readily access Ala torsions favorable to β-hairpin folding (see Supplementary Material for details).

6. Discussion

The current work once again demonstrates the enhanced β-sheet propensity of hydrazino acid residues using a distinct β-hairpin model system. In our previous examination of folded NAPs, we observed secondary structure stabilization with aTyr, aLys, and aLeu substitutions within a 12-residue β-hairpin.[6] Enhanced stability from two other hydrazino acid residues in this study (aPhe, aVal) suggests that *N*-amination may be a general strategy for promoting β-sheet folds. Polyamination along a single edge of an extended peptide appears to be a particularly powerful approach for β-strand stabilization. Peptide **14** represents the second example where strand di-*N*-amination yields a β-hairpin that is isoenergetic, in water, with its fully folded macrocyclic control. This remarkable effect is observed in spite of the presence of two tertiary amide bonds within the peptide strand. We previously attributed this result to a combination of *cis* amide rotamer destabilization, intraresidue C6 H-bonding, and enhanced torsional strain resulting from the introduction of the *N*-amino group.[6]

The data in Table 2 shed some light on the relative importance of non-covalent interactions for β-hairpin folding within this series. Although the minor *cis* amide rotamer of *N*-methylated peptide **15** is effectively unstructured, the *trans* rotamer (65% of the rotameric mixture) still exhibits poor folding relative to **4**. This is in agreement with previous data reported for **15** and suggests that other factors are primarily responsible for the strong β-hairpin destabilizing effect of *N*-methylation.[10f] The *trans*-locked motifs (pyz, tpy, tpd) in **9**–**11** were better accommodated into the β-hairpin than the *N*-methyl substituent. However, we did not observe any *cis* amide rotamers in the NMR spectra of acyclic NAPs **12**–**14**, suggesting that covalent tethering does not provide a significant entropic benefit with respect to amide isomerism.

Acyclic NAPs are known to engage in C6 intraresidue H-bonds involving the hydrazino acid NH_2 donor and the carbonyl O acceptor (see Fig. 1).[6] Such interactions in pyz- and tpy-constrained peptides would involve an analogous H-bond donor, while the enhanced acidity of the diacylhydrazide NH in tpd-constrained peptides results in superior donating capacity. Computational analysis suggests that both tpy and pyz constraints force the *N*-amino lone pair to orient toward the peptide C-terminus, increasing its potential to act instead as an H-bond acceptor. This is in stark contrast with the acyclic NAP, in which the *N*-amino lone pair remains *syn*-periplanar to the acylhydrazide N—C bond. While the *N*-amino group in the tpd motif also acts exclusively as a H-bond donor (due to N lone pair conjugation), increased ring strain relative to the acyclic NAP may hinder its ability to adopt β-sheet-like conformations.

It is also worth noting that, in contrast to acylic NAPs **12**–**14**, each of the covalently tethered motifs in **9**–**11** lacks the native Ala13 side chain. One ongoing area of investigation is the conformational impact of quaternary cyclic subunits that restore pro-(*S*) Cα substituents. Although these side chains may be important for β-sheet folding, such designs would still be forced to overcome the energetic penalties associated with cyclic constraint.

7. Conclusions

In summary, we have developed a novel tethering approach for the constraint of conformationally extended dipeptides via on-resin Mitsunobu cyclizations. The pyz and tpy subunits are derived from readily accessible building blocks and their synthesis on solid support should facilitate their use in various peptidomimetic applications. Our assessment of the β-sheet propensity of 4 distinct NAP derivatives revealed that the 6-membered tpy and tpd constraints are better accommodated into a β-hairpin strand than the pyz ring. Though all three cyclic constraints destabilize the β-hairpin relative to the parent peptide, each promoted folding relative to backbone *N*-methylation. In the current model system, mono- and di-*N*-amination significantly enhanced β-hairpin stability. These results will inform the design of additional α-hydrazino acid building blocks capable of nucleating β-sheet-like folds.

Acknowledgments

We gratefully acknowledge the National Science Foundation for funding (NSF-CHE1709927). We thank the USF Interdisciplinary NMR Facility and USF Mass Spectrometry Facility for assistance. Computer time was provided by USF Research Computing, sponsored in part by NSF MRI CHE-1531590.

A. Supplementary data

Supplementary data associated (experimental methods, compound characterization, and supplementary figures) with this article can be found, in the online version, at http://dx.doi.org/10.1016/j.bmc.2017.08.017.

References

1. Loughlin WA, Tyndall JDA, Glenn MP, Hill TA, Fairlie DP. *Chem Rev*. 2010;110:2.
2. (a) Selkoe DJ. *Nature*. 2003;426(Suppl 1):900–904;
(b) Ross CA, Poirier MA. *Nat Med*. 2004;10:S10;
(c) Knowles TP, Vendruscolo M, Dobson CM. *Nat Rev Mol Cell Biol*. 2014;15:384.
3. (a) Nassar N, Horn G, Herrmann C, Block C, Janknecht R, Wittinghofer A. *Nat Struct Biol*. 1996;3:723;
(b) Downward J. *Nat Rev Cancer*. 2003;3:11.
4. (a) Remaut H, Waksman G. *Trends Biochem Sci*. 2006;31:436;
(b) Cheng P-N, Pham JD, Nowick JS. *J Am Chem Soc*. 2013;135:5477;
(c) Watkins AM, Arora PS. *ACS Chem Biol*. 2014;9:1747.
5. (a) Khakshoor O, Nowick JS. *Curr Opin Chem Biol*. 2008;12:722;
(b) Del Valle JR. In: Lubell W, ed. *Peptidomimetics II*. Cham: Springer International Publishing; 2017:25–49.
6. Sarnowski MP, Kang CW, Elbatrawi YM, Wojtas L, Del Valle JR. *Angew Chem Int Ed*. 2017;56:2083.
7. Kang CW, Ranatunga S, Sarnowski MP, Del Valle JR. *Org Lett*. 2014;16:5434.
8. Gronenborn AM, Filpula DR, Essig NZ, et al. *Science*. 1991;253:657.
9. Blanco FJ, Rivas G, Serrano L. *Nat Struc Biol*. 1994;1:584.
10. (a) Fesinmeyer RM, Hudson FM, Andersen NH. *J Am Chem Soc*. 2004;126:7238;
(b) Huyghues-Despointes BMP, Qu X, Tsai J, Scholtz JM. *Proteins*. 2006;1005:63;
(c) Wei Y, Huyghues-Despointes BMP, Tsai J, Scholtz JM. *Proteins*. 2007;69:285;
(d) Lengyel GA, Horne WS. *J Am Chem Soc*. 2012;134:15906;
(e) Lengyel GA, Eddinger GA, Horne WS. *Org Lett*. 2013;15:944;
(f) Lengyel GA, Reinert ZE, Griffith BD, Horne WS. *Org Biomol Chem*. 2014;12:5375;
(g) Karnes MA, Schettler SL, Werner HM, Kurz AF, Horne WS, Lengyel GA. *Org Lett*. 2016;18:3902.
11. Griffiths-Jones SR, Maynard AJ, Searle MS. *J Mol Biol*. 1999;292:1051.
12. Minor DL, Kim PS. *Nature*. 1994;367:660.
13. Armstrong A, Jones LH, Knight JD, Kelsey RD. *Org Lett*. 2005;7:713.
14. Kang CW, Sarnowski MP, Elbatrawi YM, Del Valle JR. *J Org Chem*. 2017;82:1833.
15. Dekan Z, Vetter I, Daly NL, Craik DJ, Lewis RJ, Alewood PF. *J Am Chem Soc*. 2011;133:15866.
16. Fischer PM. *Tetrahedron Lett*. 1992;33:7605.
17. (a) Miller BT, Singh RP, Klauda JB, Hodošček M, Brooks BR, Woodcock HLJ. *Chem Inf Mod*. 1920;2008:48;
(b) Brooks BR, Brooks CL, Mackerell AD, et al. *J Comp Chem*. 2009;30:1545.
18. (a) Chai J-D, Head-Gordon M. *Phys Chem Chem Phys*. 2008;10:6615;
(b) Chai J-D, Head-Gordon M. *J Chem Phys*. 2008;128:084106;
(c) Shao Y, Gan Z, Epifanovsky E, et al. *Mol Phys*. 2015;113:184;
(d) Woodcock HL, Hodošček M, Gilbert ATB, Gill PMW, Schaefer HF, Brooks BR. *J Comp Chem*. 2007;28:1485.
19. Glendening ED, Landis CR, Weinhold F. *J Comp Chem*. 2013;34:1429.